

Ground-state phase diagram of the $S = 1$ one-dimensional Kondo lattice model with a uniaxial anisotropy under transverse fields

Kohei Suzuki and Kazumasa Hattori

Department of Physics, Tokyo Metropolitan University, 1-1 Minami-osawa, Hachioji, Tokyo 192-0397, Japan

We study effects of transverse magnetic fields in the $S = 1$ one-dimensional Kondo lattice model with a uniaxial anisotropy by using the density matrix renormalization group. The model can be regarded as a simplified one for analyzing an Ising ferromagnetic superconductor URhGe. We find various phases such as ferromagnetic and antiferromagnetic phases, Kondo plateau (KP) phases, the Tomonaga-Luttinger liquid, and fully-polarized phases. In the KP phase, a pseudo plateau emerges in the magnetization due to strongly-bound pairs between the local and the conduction electron spins. This is the reason why we call this phase Kondo plateau. At the critical field between the ferromagnetic and the KP phases, we find metamagnetic behavior in the magnetization curve. We discuss various correlation functions and the Friedel oscillations in details and the experimental data under transverse magnetic fields in URhGe are discussed on the basis of the present results.

1. Introduction

Coexistence of ferromagnetism (FM) and superconductivity (SC) has attracted great attention since the discovery in UGe_2 .¹⁾ Since then, some other materials showing the ferromagnetic SC have been found such as URhGe,²⁾ UIr,³⁾ and UCoGe.⁴⁾ Among them, URhGe and UCoGe have been discussed in great details in recent years.⁵⁻⁸⁾ They show SC inside their ferromagnetic state in the ambient pressure.^{2,4)} One of the common properties in the U-based ferromagnetic superconductors is their strong Ising anisotropy and strongly anisotropic magnetic fluctuations have been observed in the NMR experiments.⁹⁻¹²⁾ To clarify the relations between the SC and the Ising magnetic fluctuations is one of the important issues in these systems.

In URhGe and UCoGe, applying magnetic fields along the transverse direction (\parallel b-axis) relative to the Ising axis (c-axis) shows dramatic changes in their SC. For URhGe, the ferromagnetic phase transition takes place at $T_c \sim 9.5$ K with the magnetic moment $M_0 \sim 0.4\mu_B$ along the c-axis.²⁾ Inside the FM state, the superconductivity emerges at $T_{\text{sc}} = 0.26$ K for $H = 0$ T.²⁾ The magnetic field along the b-axis suppresses the SC and it disappears at $H \sim 2$ T. However, another SC appears for $H = 9 \sim 13$ T and the T_{sc} shows a maximum value 0.42 K for $H \sim 12$ T.⁵⁾ This is called a reentrant SC (RSC). This RSC emerges near the critical magnetic field along the b-axis, above which the FM disappears and the moment is polarized along the b-axis. Thus, the origin for the RSC would be related to the physics of the transverse-field Ising model (fluctuation); a well known model that possesses a quantum criticality.¹³⁾ Detailed experimental investigations have revealed that the transition is first order and there is a tricritical point at finite temperature,^{14, 15)} while there exists a smooth changes in the thermodynamic quantities such as the magnetization curve.¹⁶⁾ This suggests that it is a “weak” first order transition. Indeed, the magnetization strongly increases

around $H \sim 12$ T, which is typical metamagnetic behavior. This is also reflected in the relaxation time T_2 in the NMR experiment,⁹⁾ in which $1/T_2$ shows strong enhancement.

As for the theoretical analyses, several works have been done,¹⁷⁻²⁴⁾ which include SC mediated by spin-wave excitations near the critical field¹⁸⁾ and by phenomenological spin fluctuations,²³⁾ and SC near Lifshitz transitions.²⁴⁾ Inevitable line nodes in the superconducting gap functions characteristic to the nonsymmorphic zig-zag chain structure along a-axis are pointed out recently²⁵⁾ and also interesting topological SC for UCoGe is proposed.²⁶⁾

In this paper, we focus on the effects of transverse magnetic fields in the Kondo lattice model with strong Ising anisotropy. To simplify the analysis, we consider the one-dimensional model and the local spin $S = 1$. The first simplification corresponds to ignoring inter-chain couplings in URhGe and related compounds. The second one, taking $S = 1$ model, enables us to discuss the uniaxial single-ion anisotropy with keeping the essential property of the U-based ferromagnetic SCs. This is the lowest spin and the analysis becomes much simpler than that for the larger spin.

For more than two decades, a number of studies about the $S = 1/2$ Kondo lattice model have been carried out.²⁷⁻³¹⁾ In contrast, for larger spin models, including $S = 1$ one, it has not been studied in details so far. The $S = 1$ Kondo lattice model has been analyzed by means of mean-field theory in Refs. 32 and 33 for discussing U-based heavy fermions. For impurity Kondo models, the Kondo model with an $S = 1$ local spin interacting with $s = 3/2$ conduction electrons has been discussed and shown to be an exotic non-Fermi liquid.³⁴⁾ Although much attention has been paid to the SC under magnetic fields in URhGe and UCoGe, there are no study focusing on the ground-state properties and the phase diagram for microscopic models with strong Ising anisotropy in the Kondo lattice systems. Thus, it is important to analyze the $S = 1$ Kondo lattice model and to construct the phase diagram un-

der transverse fields in order to discuss the metamagnetism and possibly the RSC in URhGe. To this end, we employ the density matrix renormalization group (DMRG),³⁵⁾ which is a well-known powerful numerical tool for analyzing one-dimensional systems.

This paper is organized as follows. In Sect. 2, the model used in this study and some of the DMRG details specific to the model are introduced. Then, we will show the numerical results, which include ground-state phase diagrams and various correlation functions in Sect. 3. In Sect. 4, we will discuss our numerical results by comparing it with experimental data in URhGe, and finally, will summarize the present results.

2. Model

In this section, we will introduce the model and explain the basic properties of the model. The Hamiltonian of $S = 1$ one-dimensional Kondo lattice model with a uniaxial anisotropy D under a transverse field h is given as

$$\begin{aligned} \hat{H} = & -t \sum_{j=1}^{N-1} \sum_{\sigma=\uparrow,\downarrow} \left(\hat{c}_{j\sigma}^\dagger \hat{c}_{j+1\sigma} + \hat{c}_{j+1\sigma}^\dagger \hat{c}_{j\sigma} \right) \\ & + J \sum_{j=1}^N \hat{\mathbf{S}}_j \cdot \hat{\mathbf{S}}_j - h \sum_{j=1}^N \left(\hat{s}_j^x + \hat{s}_j^y \right) - D \sum_{j=1}^N (\hat{s}_j^z)^2. \end{aligned} \quad (1)$$

Here, $\hat{c}_{j\sigma}$ is the annihilation operator of the conduction electron at the j site with the spin $\sigma = \uparrow$ or \downarrow . $\hat{\mathbf{S}}_j = (\hat{s}_j^x, \hat{s}_j^y, \hat{s}_j^z)$ and $\hat{\mathbf{S}}_j = (\hat{s}_j^x, \hat{s}_j^y, \hat{s}_j^z)$ are the spin operators for the conduction electron and the spin-1 local spin at the j site, respectively. $J > 0$ is the antiferromagnetic Kondo exchange coupling and the nearest-neighbor hopping t is set to unity as a unit of energy. In order to represent the strong Ising anisotropy, we set $D = 1$ for simplicity in this paper. Without loss of generality, we can assume that the transverse field h is along x direction.

In the presence of h , the z -component of the total spins is not conserved. It is important to chose the bases with which the Hamiltonian (1) is block-diagonalized. For this, we need to find the operators that commute with the Hamiltonian (1). The total number operator $\hat{N}_c = \sum_{i,\sigma} \hat{c}_{i\sigma}^\dagger \hat{c}_{i\sigma}$ and the total spin inversion operator $\hat{P} = \prod_{j=1}^N \hat{P}_j$ meet this requirement. The local spin inversion operator \hat{P}_j acts on the local bases for the conduction electrons as follows:

$$\begin{aligned} \hat{P}_j |\text{vac}\rangle_j &= |\text{vac}\rangle_j, \quad \hat{P}_j |\uparrow\rangle_j = |\downarrow\rangle_j, \\ \hat{P}_j |\downarrow\rangle_j &= |\uparrow\rangle_j, \quad \hat{P}_j |\uparrow\downarrow\rangle_j = |\downarrow\uparrow\rangle_j, \end{aligned} \quad (2)$$

where $|\text{vac}\rangle_j$ indicates the empty state for the j site, $|\sigma\rangle_j = \hat{c}_{j\sigma}^\dagger |\text{vac}\rangle_j$, and $|\uparrow\downarrow\rangle_j = \hat{c}_{j\uparrow}^\dagger \hat{c}_{j\downarrow}^\dagger |\text{vac}\rangle_j$. For the local spins,

$$\hat{P}_j |\uparrow\rangle_j = |\downarrow\rangle_j, \quad \hat{P}_j |0\rangle_j = |0\rangle_j, \quad \hat{P}_j |\downarrow\rangle_j = |\uparrow\rangle_j, \quad (3)$$

where the local bases for the local spins are the eigenstates for \hat{s}_j^z : $|\uparrow\rangle_j$, $|0\rangle_j$, and $|\downarrow\rangle_j$ with the eigenvalue 1, 0, and -1 , respectively. The eigenvalues of \hat{P}_j are $P_j = \pm 1$, since $\hat{P}_j^2 = 1$. The eigenstates of \hat{P}_j for the conduction electrons are summarized

as

$$\begin{aligned} |\text{vac}\rangle_j \cdots P_j &= 1, \\ \hat{c}_{j,e}^\dagger |\text{vac}\rangle_j &:= \frac{1}{\sqrt{2}} (|\uparrow\rangle_j + |\downarrow\rangle_j) \cdots P_j = 1, \\ \hat{c}_{j,o}^\dagger |\text{vac}\rangle_j &:= \frac{1}{\sqrt{2}} (|\uparrow\rangle_j - |\downarrow\rangle_j) \cdots P_j = -1, \\ \hat{c}_{j,o}^\dagger \hat{c}_{j,e}^\dagger |\text{vac}\rangle_j &:= |\uparrow\downarrow\rangle_j \cdots P_j = -1. \end{aligned} \quad (4)$$

Here, $\hat{c}_{j,e(o)}^\dagger$ is the creation operator for the conduction electron with even (odd) parity. They are defined as

$$\hat{c}_{j,e}^\dagger = \frac{1}{\sqrt{2}} (\hat{c}_{j\uparrow}^\dagger + \hat{c}_{j\downarrow}^\dagger), \quad \hat{c}_{j,o}^\dagger = \frac{1}{\sqrt{2}} (\hat{c}_{j\uparrow}^\dagger - \hat{c}_{j\downarrow}^\dagger). \quad (5)$$

As for the eigenstates of \hat{P}_j for the local spins,

$$\begin{aligned} |\text{EV}\rangle_j &:= \frac{1}{\sqrt{2}} (|\uparrow\uparrow\rangle_j + |\downarrow\downarrow\rangle_j) \cdots P_j = 1, \\ |0\rangle_j \cdots P_j &= 1, \\ |\text{OD}\rangle_j &:= \frac{1}{\sqrt{2}} (|\uparrow\uparrow\rangle_j - |\downarrow\downarrow\rangle_j) \cdots P_j = -1. \end{aligned} \quad (6)$$

With these bases, the Hamiltonian (1) is rewritten as

$$\begin{aligned} \hat{H} = & -t \sum_{j=1}^{N-1} \sum_{p=\text{e,o}} \left(\hat{c}_{j,p}^\dagger \hat{c}_{j+1,p} + \hat{c}_{j+1,p}^\dagger \hat{c}_{j,p} \right) \\ & + J \sum_{j=1}^N \left(\hat{s}_j^x \hat{s}_j^x + \hat{s}_j^y \hat{s}_j^y + \hat{s}_j^z \hat{s}_j^z \right) - h \sum_{j=1}^N \left(\hat{s}_j^x + \hat{s}_j^y \right) \\ & - D \sum_{j=1}^N \left(1 - |\text{OD}\rangle_j \langle \text{OD}|_j \right), \end{aligned} \quad (7)$$

and the spin operators are represented in the new bases as

$$\hat{s}_j^x = \frac{1}{2} \left(\hat{c}_{j,e}^\dagger \hat{c}_{j,e} - \hat{c}_{j,o}^\dagger \hat{c}_{j,o} \right), \quad (8)$$

$$\hat{s}_j^y = \frac{i}{2} \left(\hat{c}_{j,e}^\dagger \hat{c}_{j,o} - \hat{c}_{j,o}^\dagger \hat{c}_{j,e} \right), \quad (9)$$

$$\hat{s}_j^z = \frac{1}{2} \left(\hat{c}_{j,e}^\dagger \hat{c}_{j,e} + \hat{c}_{j,o}^\dagger \hat{c}_{j,o} \right), \quad (10)$$

$$\hat{s}_j^x = |\text{EV}\rangle_j \langle \text{EV}|_j + |0\rangle_j \langle \text{EV}|_j, \quad (11)$$

$$\hat{s}_j^y = i \left(|0\rangle_j \langle \text{OD}|_j - |\text{OD}\rangle_j \langle 0|_j \right), \quad (12)$$

$$\hat{s}_j^z = |\text{EV}\rangle_j \langle \text{OD}|_j + |\text{OD}\rangle_j \langle \text{EV}|_j. \quad (13)$$

The DMRG calculations have been done in these bases in each of the subspaces specified by the electron number N_c and the total spin parity $P = \pm 1$.

Let us comment on the particle-hole symmetry. Hamiltonian (7) is invariant under the particle-hole transformation,

$$\hat{c}_{j,e} \rightarrow (-1)^j \hat{c}_{j,o}^\dagger, \quad \hat{c}_{j,o} \rightarrow (-1)^{j+1} \hat{c}_{j,e}^\dagger. \quad (14)$$

The filling of the conduction electrons n_c changes under the

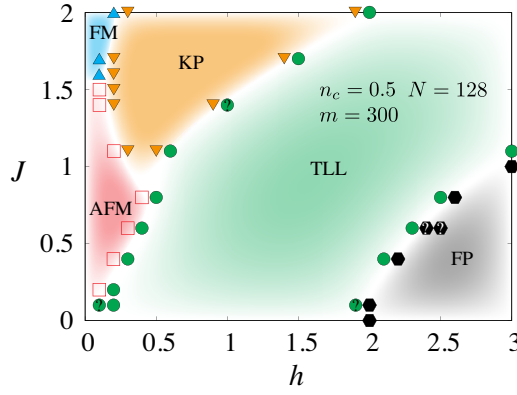


Fig. 1. Ground-state h - J phase diagram for $N = 128$ and $n_c = 0.5$. Each phase is identified by the long-distance behavior of the spin-spin correlation functions $\chi_z^{sc}(r)$ and $\chi_z^S(r)$. They do not decay and is finite in the Ising-ordered phases, while decay in the KP and FP phases. In the TLL phase, they show a power-law decay. Symbols with “?” near phase boundaries indicate that the ground state is not determined within the system sizes $N \leq 128$ and the cutoff $m = 300$.

transformation as follows:

$$n_c = \frac{N_c}{N} = \frac{1}{N} \sum_{j=1}^N \sum_{p=e,o} \langle \hat{c}_{j,p}^\dagger \hat{c}_{j,p} \rangle \rightarrow 2 - n_c, \quad (15)$$

where $\langle \hat{A} \rangle$ represents the ground-state expectation value of the operator \hat{A} . Considering Eq. (15), systems with the filling n_c are equivalent to those for $2 - n_c$ and it is sufficient to consider $n_c \leq 1$.

Since the parity index for the conduction electrons changes through Eq. (14), the total spin parity for the electrons depends on the electron number N_c . It is invariant for N_c being even, while it changes for odd. Since the particle-hole transformation does not affect the parity for the local spins, the total spin parity is invariant if N_c is even, while it changes if N_c is odd. Thus, systems for $n_c > 1$ can be trivially mapped to those for $n_c < 1$ and it is sufficient to consider $n_c \leq 1$.

3. Result

In this section, we will show the numerical results in details. DMRG calculations have been done for $N = 32, 64, 128$ and kept at least $m = 200$ states in the truncation procedures. We will mainly discuss the results for $N = 128$ and, if necessary, the N dependence will be discussed. In the following, we will first show the h - J phase diagram for $n_c = 0.5$ and then discuss the physical quantities such as the magnetizations, various correlation functions, and the critical properties.

3.1 Phase diagrams

Let us first show the ground-state h - J phase diagram determined by the DMRG method for the typical conduction electron filling $n_c = 0.5$. Here, we will explain overall features and properties of phases appearing in the diagram and will discuss various physical quantities later in this section. For other values of n_c , the results are discussed in Sect. 3.5, in which qualitatively similar phase diagrams are obtained with some new phases.

Figure 1 shows the h - J phase diagram for $n_c = 0.5$. There are various phases such as ferromagnetic (FM), antiferromagnetic (AFM), the Tomonaga-Luttinger liquid (TLL), Kondo plateau (KP) (we will explain the meaning later), and fully-polarized (FP) phases. Each of the phases shows a characteristic long-distance asymptotic dependence in the spin-spin correlation functions such as

$$\chi_z^S(r) := \langle \hat{S}_{r+N/2}^z \hat{S}_{N/2}^z \rangle, \quad \chi_z^{sc}(r) := \langle \hat{s}_{r+N/2}^z \hat{s}_{N/2}^z \rangle. \quad (16)$$

The FM and the AFM orders are Ising like and possible even in one-dimensional system at zero temperature. These phases appear for small h . In particular, the FM phase emerges for large J and small n_c (see also Sect. 3.5). The spin-spin correlation functions do not vanish as $r \rightarrow \infty$ in these phases, which is the signature of the symmetry breaking.

In the KP phase, tightly-bound local Kondo “doublets” are formed by the conduction electrons and the local spins and one of the two components gains the magnetic energy due to h . Note that the magnitudes of the local spin and the conduction electron one are different in our model. To destroy such a tightly-bound doublet needs a large magnetic field. This is reflected in the pseudo plateau in the magnetization and in the local spin-spin correlation:

$$\langle \hat{s} \cdot \hat{S} \rangle := \frac{1}{N} \sum_{j=1}^N \langle \hat{s}_j \cdot \hat{S}_j \rangle. \quad (17)$$

We call this phase “Kondo plateau” after these observations. As will be discussed in Sect. 3.3, the spin-spin correlation functions (16) decay exponentially for $r \rightarrow \infty$, which indicates the spin excitations have a finite gap.

In a wide range of parameter space, there appears the TLL phase, where the spin-spin correlation functions exhibit power-law decay, which indicates the quasi long-range order. Strictly speaking, it is “TLL” for the charge sector in other phases, but we here use the name TLL in order to distinguish this phase and others by focusing on the spin sector only. For sufficiently high fields, the FP state appears and this phase is a trivial one expected in the band-shift picture due to the external magnetic field h .

3.2 Magnetization curve and Kondo correlations

Now, we discuss the response of the ground state against the external transverse magnetic field h . One of the most relevant quantities for experimental studies is the magnetization and let us start to discuss this.

Figure 2 shows the magnetizations along the x -direction,

$$M_x = \frac{1}{N} \sum_{j=1}^N \langle \hat{S}_j^x \rangle, \quad m_x = \frac{1}{N} \sum_{j=1}^N \langle \hat{s}_j^x \rangle, \quad (18)$$

as a function of h for several values of J for $n_c = 0.5$. M_x is induced as h increases and around $h \sim 3.0$, the moment reaches the saturated value 1 for all J 's. We note that for larger J , $J = 2.0$ and $J = 1.5$, M_x exhibits non-monotonic h dependence. For example, for $J = 2.0$, below $h = h_{KP} \simeq 1.92$, M_x monotonically increases as if the full moment were ~ 0.8 and

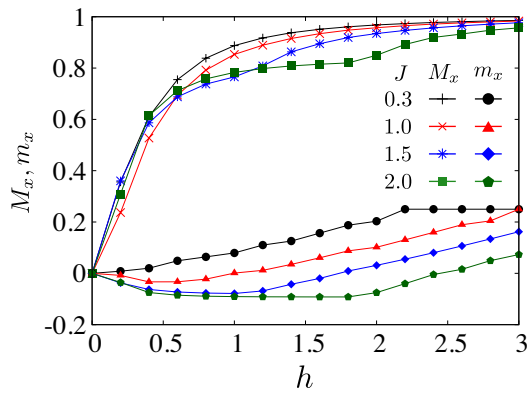


Fig. 2. h dependence of M_x and m_x for $J = 0.3, 1.0, 1.5$, and 2.0 , and $N = 128$, $n_c = 0.5$ with the cutoff $m = 200$. M_x is for the local spins and m_x for the conduction electrons. [See eq. (18)]

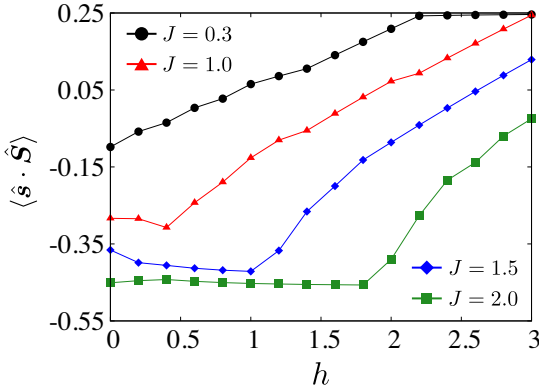


Fig. 3. h dependence of $\langle \hat{s} \cdot \hat{S} \rangle$, the correlation between the local spins and the electron spins, for $J = 0.3, 1.0, 1.5$, and 2.0 , and $N = 128$, $n_c = 0.5$ with the cutoff $m = 200$.

exhibits (almost) no h dependence between $h \sim 1$ and h_{KP} . Correspondingly, m_x decreases for small h and is almost constant with a negative value. In contrast to the case of $J = 0.3$, it increases and reaches the saturated value $1/4$ at $h \simeq 2.2$. Note that m_x for large J starts to increase also at $h = h_{\text{KP}}$.

In order to understand this non-monotonic h dependence, we analyze the correlation between the conduction electron spins and the local spins: $\langle \hat{s} \cdot \hat{S} \rangle$ [Eq. (17)]. Figure 3 shows the h dependence of $\langle \hat{s} \cdot \hat{S} \rangle$. For $J = 2.0$, $\langle \hat{s} \cdot \hat{S} \rangle \simeq -0.45$ and this means the electron and the local spin are almost frozen, forming an anti-parallel configuration, which can be also visible in Fig. 2. Since the magnitudes of the two are different, there remains a residual moment. This residual moment aligns along the external field h , leading to the positive M_x and the negative m_x in Fig. 2, since the residual moment is parallel to the local spin. This indicates that the plateau in M_x is due to the strong Kondo correlations; the “spin molecule” is formed between the conduction electrons and the local spins. Above h_{KP} , this molecule is resolved and M_x , m_x , and $\langle \hat{s} \cdot \hat{S} \rangle$ start to increase. The transition at $h = h_{\text{KP}}$ separates the KP and the TLL phases. Unfortunately, it is hard to judge whether the transition is first- or second-order in the present calculations

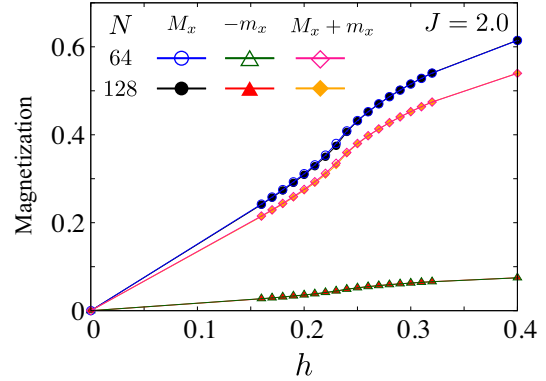


Fig. 4. Magnetizations M_x and m_x as a function of h near the phase boundary between the FM and the KP phases for $J = 2.0$, $N = 64$, 128 , and $n_c = 0.5$ with the cutoff $m = 200$. Note that $-m_x$ (triangles) is plotted for the conduction electron.

for $N = 128$ and $m = 300$; the correlation lengths of the spin-spin correlation functions are finite at $h = h_{\text{KP}}$, while M_x , m_x , and $\langle \hat{s} \cdot \hat{S} \rangle$ exhibit no signature of discontinuity at $h = h_{\text{KP}}$ in their N dependence.

At low fields, there is another phase transition that separates the KP and the Ising-ordered phases for $J = 2.0$ and 1.5 . Figure 4 shows the low-field magnetization curve near the transition. The phase boundary corresponds to the field where the M_x shows a (metamagnetic like) steep increase as a function of the field; $h_c \sim 0.24$ for $J = 2.0$. Although it is not a direct evidence for the phase transition, it suggests there is some anomaly at $h = h_c$. We will discuss this point in Sect. 3.3 by analyzing correlation functions and the low-field phase turns out to be an Ising FM for $J = 2.0$ and 1.5 . For smaller $J = 0.3$, there is no KP phase and there is one transition from the Ising AFM to the TLL phases as h increases. For $J = 1.0$, it seems there is a small region of the KP phase between the FM and the TLL phases around $h = 0.4$ (see Figs. 2 and 3).

3.3 Correlation functions

As discussed above, there are various phases as functions of J and h . In order to clarify the nature of each phase, analyzing the correlation functions, e.g., Eq. (16), is important. One can unveil the spatial modulation and the long-distance asymptotic behavior by examining appropriate correlation functions.

The Ising-ordered phases are stabilized for small h . When J is large, the FM phase appears and $\chi_z^S(r)$ and $\chi_z^{sc}(r)$ [Eq. (16)] exhibit long-range correlations. The magnetization along the z -direction is estimated as $M_z^2 = \lim_{r \rightarrow \infty} \chi_z^S(r)$ and $m_z^2 = \lim_{r \rightarrow \infty} \chi_z^{sc}(r)$. Figure 5 shows the r dependence of $\chi_z^S(r)$ and $\chi_z^{sc}(r)$ for $h = 0.2$ and $J = 2.0$, i.e., in the FM phase. One can see that $\chi_z^S(r)$ and $\chi_z^{sc}(r)$ do not decay for long distance except for the effect of the open boundary condition, which indicates the system is in the FM state. As shown in Fig. 3, $\langle \hat{s} \cdot \hat{S} \rangle$ is negative, which means that the local spins and conduction electron ones are anti-parallel with each other due to the strong Kondo exchange coupling J . This kind of FM phase was also found in $S = 1/2$ Kondo lattice model.²⁷⁾ In order to gain the kinetic energy for the conduction electrons, the conduction electrons hop to the neighboring sites with their

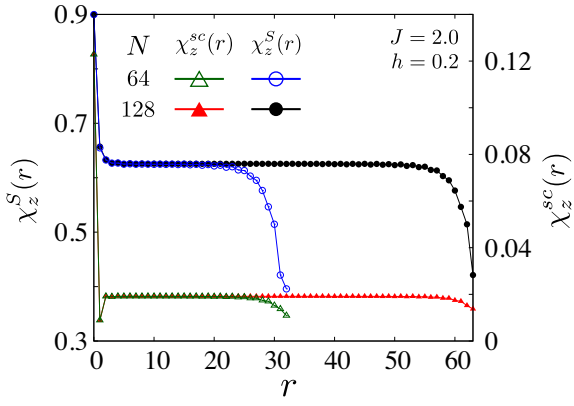


Fig. 5. r dependence of the spin-spin correlation functions $\chi_z^S(r)$ and $\chi_z^{sc}(r)$ for $N = 64$ and 128 inside the FM phase: $J = 2.0$, $h = 0.2$, and $n_c = 0.5$ with the cutoff $m = 200$. The suppression for $r \sim N/2$ is due to the boundary effects.

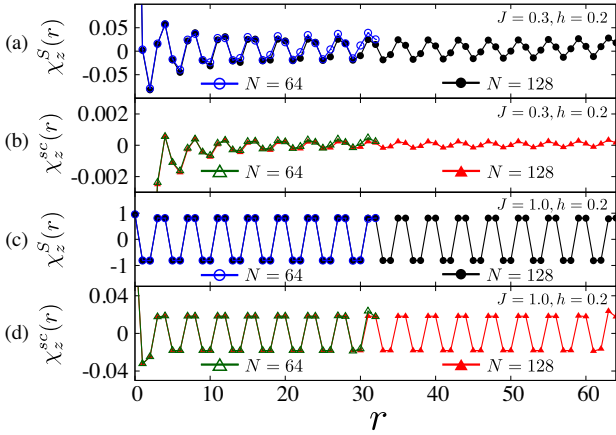


Fig. 6. r dependence of the spin-spin correlation functions for $N = 64$ (open symbols), 128 (filled symbols), and $n_c = 0.5$ with the cutoff $m = 200$: (a) $\chi_z^S(r)$ for $(J, h) = (0.3, 0.2)$, (b) $\chi_z^{sc}(r)$ for $(J, h) = (0.3, 0.2)$, (c) $\chi_z^S(r)$ for $(J, h) = (1.0, 0.2)$, and (d) $\chi_z^{sc}(r)$ for $(J, h) = (1.0, 0.2)$. One can see “up-up-down-down” structure.

spins antiparallel to the local ones.³⁶⁾ Actually, the FM phase is stabilized for small filling, since the conduction electrons are easy to traverse. See also Sect. 3.5 for the phase diagrams for $n_c \neq 0.5$.

For small J and h , the AFM phase appears. Figures 6(a) and 6(b) show the r dependence of $\chi_z^S(r)$ and $\chi_z^{sc}(r)$, respectively, for $J = 0.3$ and $h = 0.2$. $\chi_z^S(r)$ shows four-site periodicity structure and no decay for large r . This structure becomes clearer and shows “up-up-down-down” structure as J increases as shown in Figs. 6(c) and 6(d) for $J = 1.0$. The main origin for this AFM state is expected to be the RKKY interactions.^{37–39)} When the Kondo interaction J is small, the J term can be regarded as a perturbation, and thus, the lowest-order interaction between the local spins is the RKKY interaction mediated by conduction electrons. Consider the weak-coupling limit, since $D = 1 \gg J$, the large D prohibits the local spin from flipping by ± 1 and it leads to the Ising-like interaction between the local spins J_{eff} as

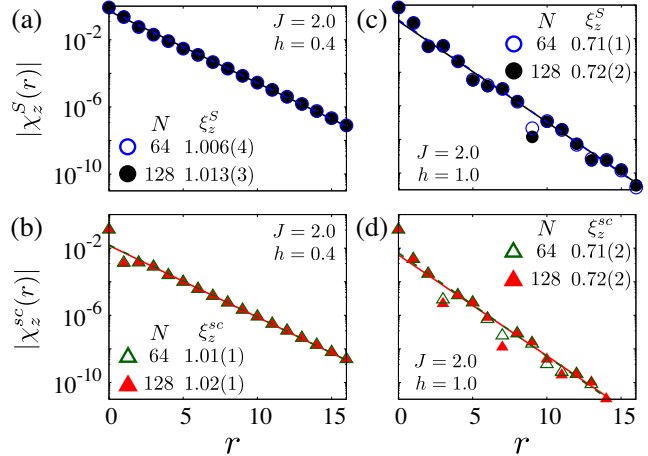


Fig. 7. r dependence of the spin-spin correlation functions for $N = 64$ (open symbols), 128 (filled symbols), and $n_c = 0.5$ with the cutoff $m = 200$ in the KP phase: (a) $|\chi_z^S(r)|$ for $(J, h) = (2.0, 0.4)$, (b) $|\chi_z^{sc}(r)|$ for $(J, h) = (2.0, 0.4)$, (c) $|\chi_z^S(r)|$ for $(J, h) = (2.0, 1.0)$, and (d) $|\chi_z^{sc}(r)|$ for $(J, h) = (2.0, 1.0)$. The dashed lines represent the fit by $A \exp(-r/\xi_z^{S, sc})$ for $N = 128$ (64), where A and $\xi_z^{S, sc}$ are the fitting parameters.

$$J_{\text{eff}}(q) \sim \left(J + \frac{J^2}{2D} \right)^2 \chi_{z0}^{sc}(q). \quad (19)$$

Here, $\chi_{z0}^{sc}(q)$ represents the z component of the static spin susceptibility with the wavenumber q for the non-interacting conduction electrons. The dominant Fourier component of (19) is one with $q = 2k_{F0}$, where k_{F0} is the Fermi wavenumber for $J = h = 0$. Thus, it is natural to expect that the period of the oscillation in $\chi_z^S(r)$ corresponds to the inverse of $2k_{F0}$. Indeed, when $n_c = 1/2$ and $h = 0$, the wavelength is estimated as $2\pi/(2k_{F0}) \sim 2/n_c = 4$, which is consistent with the “up-up-down-down” structure as shown in Fig. 6. Since $\chi_z^{S, sc}(r)$ is related to the inter-band spin fluctuations under a finite h , this argument (by setting $h = 0$) is qualitatively valid for $h > 0$.

Now, we discuss the phases with a gap in the spin sector. In general, when a target sector possesses a finite excitation gap, the corresponding correlation function $\chi(r)$ decays exponentially as $r \rightarrow \infty$. The magnitude of the gap is characterized by the correlation length ξ defined by $\chi(r) \sim \exp(-r/\xi)$. In our phase diagram Fig. 1, there are three types of such gapped states. One is the FP phase, which is a trivial state for high magnetic fields. The second is the KP phase and the third is the Ising-ordered FM and AFM phases as discussed previously.

Let us first discuss the first one: the FP phase. When h is much larger than all the other parameters t , J , and D , the lower conduction electron band split by h is filled with N_c electrons (we are considering the case with $n_c \leq 1$). Flipping a single spin generates inter-band excitations and needs a finite energy $\sim h$. Thus, since $\chi_z^{sc}(r)$ measures the transverse spin excitations with respect to the direction parallel to h in the x -direction, $\chi_z^{sc}(r)$ should decay exponentially.

Second, as for the KP phase, the direction of the local and the electron spins is opposite and they form spin molecules

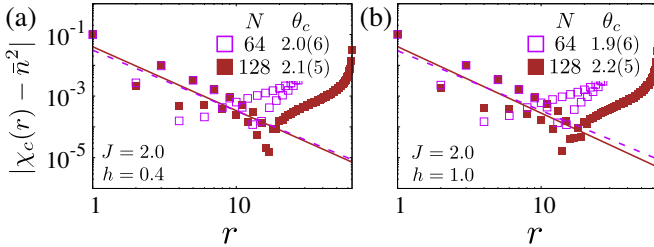


Fig. 8. r dependence of the charge correlation function $|\chi_c(r) - \bar{n}^2|$ for $N = 64$ (open symbols), 128 (filled symbols), $n_c = 0.5$ with the cutoff $m = 200$ in the KP phase: (a) $(J, h) = (2.0, 0.4)$ and (b) $(J, h) = (2.0, 1.0)$. \bar{n}^2 is estimated from the mean value of $\chi_c(r)$ for $r = 20$ to 25 for $N = 64$ and $r = 31$ to 40 for $N = 128$. The (dashed) lines represent the fit by $Ar^{-\theta_c}$ for $N = 128$ (64) in the range $r \in [1, 10]$.

due to the large J as discussed in Sect. 3.2. Thus, flipping either local or conduction electron spins needs a finite energy corresponding to the bound-state energy for the molecule. Figures 7(a) and 7(b) [7(c) and 7(d)] show the r dependence of $\chi_z^S(r)$ and $\chi_z^{sc}(r)$, respectively, for $(J, h) = (2.0, 0.4)$ [$(2.0, 1.0)$] in the KP phase. The linear decay in the semi-log plot means that $\chi_z^S(r)$ and $\chi_z^{sc}(r)$ decay exponentially. By fitting the data, we obtain the correlation lengths ξ_z^S and ξ_z^{sc} ; they are similar and $\xi_z^S \simeq \xi_z^{sc}$ for these parameter sets. This is naturally understood by noting that the correlation lengths are determined by the spin molecules “strength”. Figure 8 shows the r dependence of the charge correlation function $\chi_c(r)$, which is defined as

$$\chi_c(r) := \langle \hat{n}_{r+N/2} \hat{n}_{N/2} \rangle. \quad (20)$$

It decays to a constant value \bar{n}^2 up to $r \sim 10$ and for larger r , the data are masked by the boundary effects. Apart from this boundary effect, it is scaled as $\chi_c(r) - \bar{n}^2 \sim 1/r^{\theta_c}$. Note that \bar{n}^2 is a fitting parameter here and $\bar{n}^2 \neq n_c^2$. Thus, in the present numerical calculations, there is no evidence for the charge density wave in the KP phase for $n_c = 0.5$.

Finally, we discuss the third: the Ising-ordered states, focusing on the universality class of the phase transition between the FM and the KP phases. The h dependence of the correlation length ξ_z^S and the magnetization M_z around the phase boundary suggest that the transition belongs to the two-dimensional (2d) Ising universality class. Figure 9 shows the h dependence of M_z and ξ_z^S of $\chi_z^S(r)$ for $J = 2.0$. One can see that

$$M_z \simeq (h_c - h)^{\frac{1}{8}}, \quad \xi_z^S \simeq \frac{1}{h - h_c}, \quad \text{with } h_c \sim 0.23 - 0.24. \quad (21)$$

These dependence correspond to $\beta = 1/8$ and $\nu = 1$ in the 2d-Ising class, which is consistent with the fact that the system possesses the Ising anisotropy. The critical field $h_c \sim 0.23 - 0.24$ is consistent with the metamagnetic field observed in the magnetization in Fig. 4.

Let us close the discussion about correlation functions by examining them in the TLL phase. Figure 10 shows the r dependence of $\chi_z^S(r)$, $\chi_z^{sc}(r)$, and $\chi_c(r)$ for $(J, h) = (2.0, 2.0)$ and $(2.0, 3.0)$. The results indicate the power-law decay $\sim 1/r^\theta$, although the numerical accuracy is not sufficient for the pre-

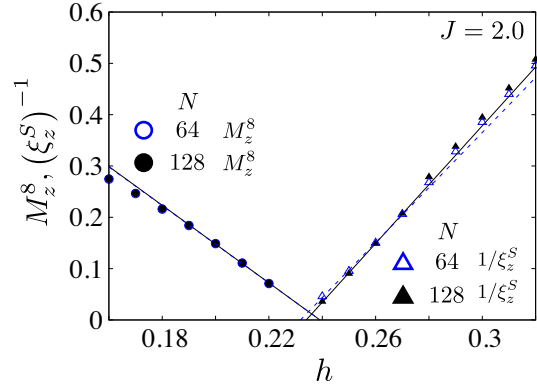


Fig. 9. h dependence of M_z^8 and $1/\xi_z^S$ for $J = 2.0$ and $n_c = 0.5$. Results are obtained from a linear extrapolation to the cutoff $m \rightarrow \infty$, by using $m = 100, 150, 200$ and 300 . The (dashed) lines represent the linear fits for M_z^8 and $1/\xi_z^S$ for $N = 128$ (64). The fittings are carried out for $h = 0.19 \sim 0.22$ for M_z^8 and for $h = 0.24 \sim 0.27$ for $1/\xi_z^S$. $M_z \sim (h_c - h)^{1/8}$ and $\xi_z^S \sim (h - h_c)^{-1}$ suggest the 2d Ising universality class.

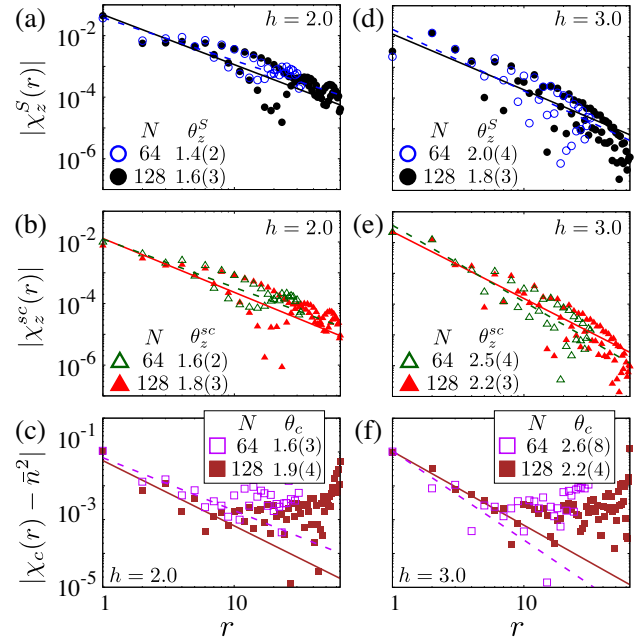


Fig. 10. r dependence of the spin-spin and the charge correlation functions for $N = 64$ (open symbols), 128 (filled symbols), and $n_c = 0.5$ with the cutoff $m = 200$ in the TLL phase: (a) $|\chi_z^S(r)|$, (b) $|\chi_z^{sc}(r)|$, and (c) $|\chi_c(r) - \bar{n}^2|$ for $(J, h) = (2.0, 2.0)$, and (d) $|\chi_z^S(r)|$, (e) $|\chi_z^{sc}(r)|$, and (f) $|\chi_c(r) - \bar{n}^2|$ for $(J, h) = (2.0, 3.0)$. The (dashed) lines represent the fit by $Ar^{-\theta}$ for $N = 128$ (64). The range of the fitting for $|\chi_c(r) - \bar{n}^2|$ is the same as that of Fig. 8 (KP phase).

cise determination of the exponent θ . For this, we need more elaborate calculations and this is one of our future problems.

3.4 Friedel Oscillations

We here analyze the spatial dependence of the expectation values: $M_j^x := \langle \hat{S}_j^x \rangle$ and $m_j^x := \langle \hat{s}_j^x \rangle$. Their spatial dependence affected by the presence of the edges shows characteristic oscillations and decay, which reflect the ground state of the system. This is known as the Friedel oscillations.⁴⁰⁾

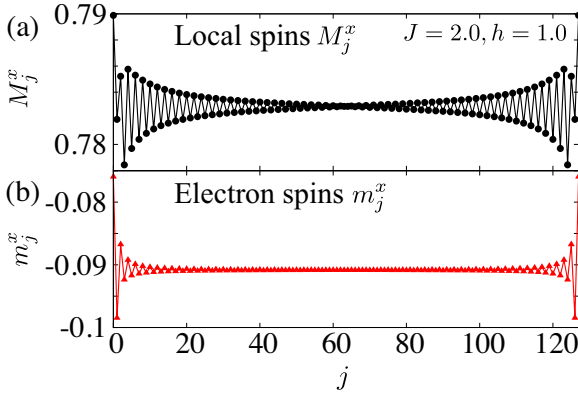


Fig. 11. Spatial dependence of the magnetizations (a) M_j^x and (b) m_j^x for $N = 128$, $J = 2.0$, $h = 1.0$, and $n_c = 0.5$ with the cutoff $m = 200$ in the KP phase. The oscillations decay exponentially to $j = 64$ from both left and right edges. The correlation lengths ξ_x^S and ξ_x^{SC} are strongly size dependent. See the main text.

Figures 11(a) and 11(b) show the spatial dependence of M_j^x and m_j^x , respectively, for $J = 2.0$ and $h = 1.0$ in the KP phase. The oscillations of these local magnetizations seem to decay exponentially toward the middle of the chain. By fitting the data in a form $\tilde{m} + c \exp(-j/\xi_x)$ for $20 < j < 40$, we can estimate the correlation length ξ_x . We find $\xi_x^S = 10.20$ for M_j^x and $\xi_x^{SC} = 8.09$ for m_j^x for $N = 64$ and $\xi_x^S = 19.46$ and $\xi_x^{SC} = 16.95$ for $N = 128$; about twice the length of that for $N = 64$. This suggests that the system size is much smaller than $\xi_x^{S,SC}$. Concerning that the system is metallic, it is natural to expect that the longitudinal fluctuation is not gapped, i.e., $\xi_x^{S,SC} \rightarrow \infty$ in the thermodynamic limit.

When the system is critical, the profile of the oscillation drastically changes. Figures 12(a) and 12(b) show M_j^x and m_j^x , respectively, for $J = 2.0$ and $h = 3.0$, where the system is in the TLL phase. The long-range oscillation, which is one of the characteristics of TLL, is induced by the presence of the edges. The dominant components of this oscillation correspond to two kinds of Fermi wavenumbers $k_{F\pm}$, where $+$ ($-$) indicates the upper (lower) conduction electron band. For $J = 0$, they are given as

$$k_{F0}^\pm(h) = \frac{\pi n_c}{2} \mp \arcsin \frac{h}{4 \sin \frac{\pi n_c}{2}}. \quad (22)$$

Suppose the Fermi surface (point) is “small” as expected for $S = 1$ Kondo lattice model,^{41,42)} $k_{F\pm}$ is identical to k_{F0}^\pm . Absolute values of the Fourier transform m_q^x of m_j^x for $h = 0.6$, 1.0, and 1.4 with fixed $J = 0.3$ are shown in Fig. 13. There are two peaks for all the three h ’s. For example, for $h = 0.6$, the two peaks locate at $q_1 = 1.28$ and $q_2 = 1.86$, which are very close to $2k_{F0}^+(h_{\text{eff}}) = 1.31$ and $2k_{F0}^-(h_{\text{eff}}) = 1.83$. Here, $h_{\text{eff}} = h - JM_x(h = 0.6) = 0.37$ is the effective field for the conduction electrons. Similarly, for $h = 1.0$ and 1.4, there are two peaks corresponding to $2k_{F0}^\pm(h_{\text{eff}})$. This is consistent with the “small Fermi surface”. For larger J , the analysis based on h_{eff} does not work and the spin correlations are not governed by the Fermi points.

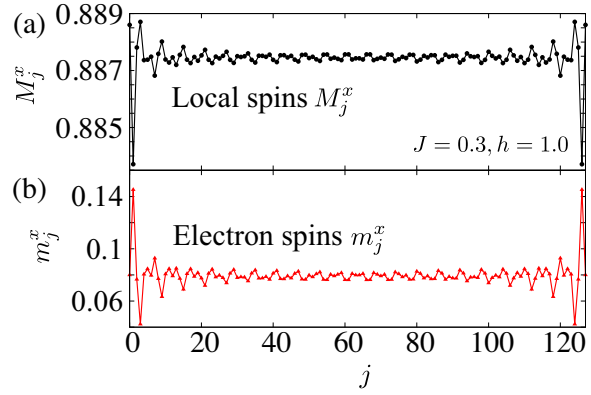


Fig. 12. Spatial dependence of the magnetizations (a) M_j^x and (b) m_j^x for $N = 128$, $J = 0.3$, $h = 1.0$, and $n_c = 0.5$ with the cutoff $m = 200$ in the TLL phase. The amplitude of the oscillations are so small that it is impossible to judge whether they show exponential or power-low decay.

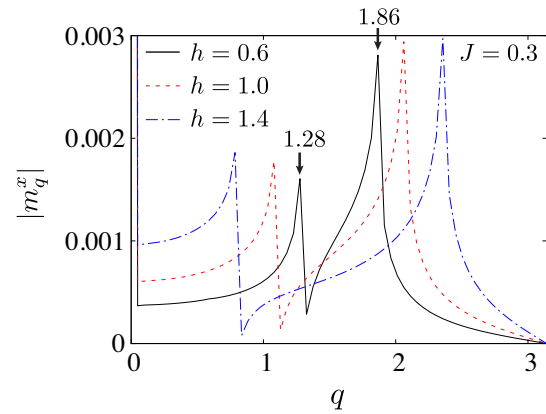


Fig. 13. Wavenumber q dependence of $|m_q^x|$ for $N = 128$, $J = 0.3$, and $n_c = 0.5$ with the cutoff $m = 200$. Data for three sets of the magnetic fields ($h = 0.6$, 1.0, and 1.4) are shown for clarity and the two peaks in each h correspond to $2k_{F\pm}$. Note that there is a large $q = 0$ component, since m_x is induced by h .

3.5 Filling dependences

So far, we have discussed the case for $n_c = 0.5$. In this subsection, we will briefly show the results for other fillings $n_c = 0.25, 0.75$, and 1.0 , since most of the phases appearing in $n_c \neq 0.5$ are similar to those appearing for $n_c = 0.5$. One qualitatively different point from $n_c = 0.5$ is that there appears a charge density wave (CDW) state in the KP and the AFM phases for $n_c = 0.75$.

Figures 14(a), 14(b), and 14(c) show the h - J phase diagrams for $n_c = 0.25, 0.75$, and 1.0 , respectively. For the smallest filling $n_c = 0.25$, the FM phase appears for the most part of the Ising-ordered phases and the KP and the FP phases occupy the wide range of the phase diagram as shown in Fig. 14(a). While for the larger fillings, the FM phase disappears and the AFM phase extends for larger h compared with the smaller fillings. In particular, for $n_c = 1.0$ [Fig. 14(c)], the AFM phase appears for intermediate fields and covers the KP phase. When $J = 0$ and $n_c = 0.75$, the FP phase appears for $h \gtrsim 3.62$ and for $n_c = 1.0$, $h > 4$.

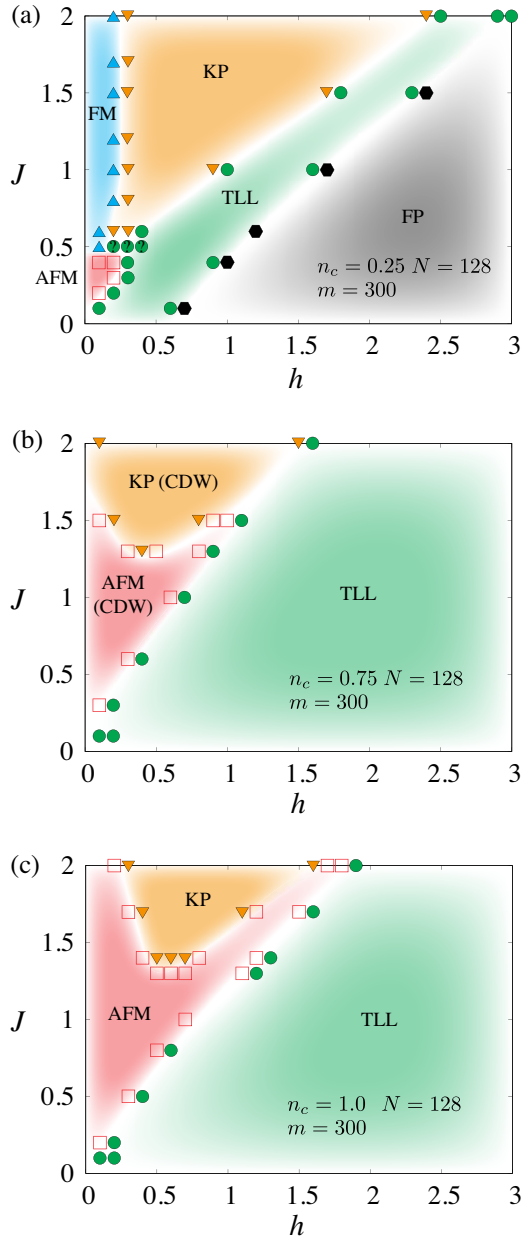


Fig. 14. Ground-state h - J phase diagram for (a) $n_c = 0.25$, (b) $n_c = 0.75$, and (c) $n_c = 1.0$. The phases are determined by analyzing the behavior of susceptibilities for $N = 64$ and 128 with the cutoff $m = 300$. Symbols represent points where numerical calculations have been done and their type and color distinguish the ground state. For clarity, only symbols near phase boundaries are indicated. Symbols with “?” near phase boundaries indicate that the ground state is not determined within the system sizes and the cutoff mentioned above. For (b) and (c), FP phase locates for $h > 3$.

As mentioned above, the CDW coexists with the AFM and the KP states for $n_c = 0.75$ in Fig. 14(b). Figure 15(a) shows the r dependence of the charge correlation function $\chi_c(r)$ for $J = 1.3$ and $h = 0.6$ in the AFM phase. One can see the oscillation with the wavenumber $q = \pi/2$. This is verified by the direct Fourier transform as shown in Fig. 15(b). Such oscillation is also found in the KP phase. Although the four-site periodicity is understandable in a sense that the filling is “3/4”, it is unclear why CDW happens only for $n_c = 0.75$. In

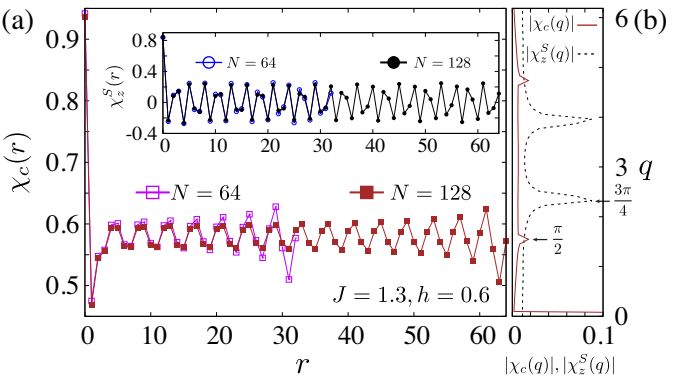


Fig. 15. Comparison between the charge and spin correlations in the AFM phase for $n_c = 0.75$, $J = 1.3$, and $h = 0.6$ with the cutoff $m = 300$. (a) Spatial dependence of $\chi_c(r)$. Inset: $\chi_z^S(r)$ as a function of r . (b) Fourier transform $\chi_c(q)$ and $\chi_z^S(q)$ for $\chi_c(r)$ and $\chi_z^S(r)$, respectively.

contrast to χ_c , the spin correlations χ_z^S and χ_z^{sc} are governed by the $2k_F$ fluctuations as discussed before. The inset of Fig. 15(a) shows $\chi_z^S(r)$ and there are complex modulations. The main Fourier mode is $q = 3\pi/4$ as shown in Fig. 15(b), which is $2k_F$ for $h = 0$. In two- and infinite-dimensional spin-1/2 Kondo lattice models, CDWs are reported at finite temperatures for $n_c \simeq 0.5$.^{30,43)} In our DMRG study, there is no evidence for the CDW for $n_c = 0.5$ and other fillings $\neq 0.75$. More detailed and sophisticated investigations⁴⁴⁾ are needed to gain a deep understanding about emergence of such CDW states.

4. Discussions and Summary

4.1 Comparison with the experimental results in URhGe

In this section, we compare our results with the experimental results in URhGe. We have studied the simplified one-dimensional model (1), keeping the ferromagnetic superconductor in URhGe in mind. In URhGe, as the external magnetic field H is applied to the hard axis (b-axis), the SC disappears at $H \sim 2$ T once, but it reappears for $H = 9 \sim 13$ T. In particular, the transition temperature T_{sc} is highly enhanced and has a maximum value 0.42 K for $H = H_R \sim 12$ T. This enhancement in T_{sc} is closely related to the spin reorientation at H_R and also to metamagnetism¹⁶⁾ originated from the tricriticality.^{14,15)}

In our model, there appears metamagnetic enhancement of M_x around h_c as shown in Fig. 4. This is in sharp contrast to the spin-wave analysis in Ref. 18, where the longitudinal magnetization is essentially given by that for the mean-field approximation. In DMRG, quantum fluctuations are fully taken into account and this is necessary for the metamagnetic behavior in Fig. 4. In the experimental situation, the tricritical point locates at $T \sim 2 \sim 4$ K^{14,15) > T_{sc} . Thus, the SC dome should be across the first-order line. One might wonder why the superconductivity is induced by the first-order transition, since the fluctuations are usually small. However, NMR experiment^{9,10)} has revealed that there is strong fluctuation even in such a situation due to the proximity to the tricritical point. As analyzed in details in Sect. 3.3, the phase transition be-}

tween the Ising FM and the KP phases are second order with the 2d Ising class. Thus, there is no tricritical point in our model. Nevertheless, it is interesting to examine whether SC fluctuations are enhanced or not and also which channels of SC are favored near the phase boundary in future studies. It is noted that there is always the TLL phase next to the FP phase in the low field side and also the high-field boundary of the FM faces the KP phase, which represents strong Kondo correlations, for parameter sets we have examined. Thus, various phases compete near the FM phase under transverse fields in the present Kondo lattice model. Generally, in such a situation, there are various fluctuations and it is interesting to examine the possibility of enhanced superconducting fluctuations. We expect such situation can capture the physics of URhGe under the transverse fields.

4.2 Summary

We have analyzed the $S = 1$ one-dimensional Kondo lattice model with a uniaxial anisotropy under a transverse field h by using DMRG, which is a simplified model for U-based ferromagnetic superconductors URhGe and related compounds under the transverse fields. We have constructed the ground-state phase diagram as functions of the magnetic field h and the Kondo exchange coupling J for several conduction electron fillings. The phase diagram includes various phases such as the Ising-ordered FM and AFM phases, the TLL, and the FP phase. In addition to them, there appears a (spin) gapped phase in moderate h between the FM and the TLL states, where the local and conduction electron spins are tightly bound antiferromagnetically and the magnetization there shows a plateau-like h dependence. We have dubbed this as Kondo plateau phase. We have also discussed the metamagnetic behavior, when the FM state is destabilized by applying the transverse field h and found a steep increase in the magnetization near the critical field for the FM. This behavior is consistent with magnetization data for URhGe. Examining the superconducting fluctuation near the critical field is an interesting future direction and is now in progress.

Acknowledgment

This work was supported by a Grant-in-Aid for Scientific Research (Grant Nos. 16H01079, 18K03522) from the Japan Society for the Promotion of Science.

- 1) S. S. Saxena, P. Agarwal, K. Ahilan, F. M. Grosche, R. K. W. Haselwimmer, M. J. Steiner, E. Pugh, I. R. Walker, S. R. Julian, P. Monthoux, G. G. Lonzarich, A. Huxley, I. Sheikin, D. Braithwaite, and J. Flouquet, *Nature* **406**, 587 (2000).
- 2) D. Aoki, A. Huxley, E. Ressouche, D. Braithwaite, J. Flouquet, J. P. Brison, E. Lhotel, and C. Paulsen, *Nature* **413**, 613 (2001).
- 3) T. Akazawa, H. Hidaka, T. Fujiwara, T. C. Kobayashi, E. Yamamoto, Y. Haga, R. Settai and Y. Ōnuki, *J. Phys. Condens. Matter* **16**, L29 (2004).
- 4) N. T. Huy, A. Gasparini, D. E. de Nijs, Y. Huang, J. C. P. Klaasse, T. Gortenmulder, A. de Visser, A. Hamann, T. Görlach, and H. v. Löhneysen, *Phys. Rev. Lett.* **99**, 067006 (2007).
- 5) F. Lévy, I. Sheikin, B. Grenier and A. D. Huxley, *Science* **309**, 1343 (2005).
- 6) A. Miyake, D. Aoki, and J. Flouquet, *J. Phys. Soc. Jpn.* **77**, 094709 (2008).
- 7) E. Hassinger, D. Aoki, G. Knebel and J. Flouquet, *J. Phys. Soc. Jpn.* **77**, 073703 (2008).
- 8) D. Aoki, T. D. Matsuda, V. Taufour, E. Hassinger, G. Knebel, and J. Flouquet, *J. Phys. Soc. Jpn.* **78**, 113709 (2009).
- 9) Y. Tokunaga, D. Aoki, H. Mayaffre, S. Krämer, M.-H. Julien, C. Berthier, M. Horvatić, H. Sakai, S. Kambe, and S. Araki, *Phys. Rev. Lett.* **114**, 216401 (2015).
- 10) Y. Tokunaga, D. Aoki, H. Mayaffre, S. Krämer, M.-H. Julien, C. Berthier, M. Horvatić, H. Sakai, T. Hattori, S. Kambe, and S. Araki, *Phys. Rev. B* **93**, 201112 (2016).
- 11) T. Hattori, Y. Ihara, Y. Nakai, K. Ishida, Y. Tada, S. Fujimoto, N. Kawakami, E. Osaki, K. Deguchi, N. K. Sato, and I. Satoh, *Phys. Rev. Lett.* **108**, 066403 (2012).
- 12) T. Hattori, K. Karube, K. Ishida, K. Deguchi, N. K. Sato, and T. Yamamura, *J. Phys. Soc. Jpn.* **83**, 073708 (2014).
- 13) S. Sachdev, *Quantum Phase Transitions* (Cambridge University Press, Cambridge, 1999) p. 39.
- 14) A. Gourgout, A. Pourret, G. Knebel, D. Aoki, G. Seyfarth, and J. Flouquet, *Phys. Rev. Lett.* **117**, 046401 (2016).
- 15) H. Kotegawa, K. Fukumoto, T. Toyama, H. Tou, H. Harima, A. Harada, Y. Kitaoka, Y. Haga, E. Yamamoto, Y. Ōnuki, Kohei M. Itoh, and E. E. Haller, *J. Phys. Soc. Jpn.* **84**, 054710 (2015).
- 16) F. Hardy, D. Aoki, C. Meingast, P. Schweiss, P. Burger, H. v. Löhneysen, and J. Flouquet, *Phys. Rev. B* **83**, 195107 (2011).
- 17) V. P. Mineev, *Phys. Rev. B* **83**, 064515 (2011).
- 18) K. Hattori and H. Tsunetsugu, *Phys. Rev. B* **87**, 064501 (2013).
- 19) C. Lörsscher, J. Zhang, Q. Gu, and R. A. Klemm, *Phys. Rev. B* **88**, 024504 (2013).
- 20) V. P. Mineev, *Phys. Rev. B* **90**, 064506 (2014).
- 21) V. P. Mineev, *Phys. Rev. B* **91**, 014506 (2015).
- 22) V. P. Mineev, *Phys. Rev. B* **96**, 104501 (2017).
- 23) Y. Tada, S. Takayoshi, and S. Fujimoto, *Phys. Rev. B* **93**, 174512 (2016).
- 24) Y. Sherkunov, A. V. Chubukov, and J. J. Betouras, *arXiv: 1805.02949*.
- 25) T. Nomoto and H. Ikeda, *J. Phys. Soc. Jpn.* **86**, 023703 (2017).
- 26) A. Daido, T. Yoshida, and Y. Yanase, *arXiv: 1803.07786*.
- 27) H. Tsunetsugu, M. Sigrist, and K. Ueda, *Rev. Mod. Phys.* **69**, 809 (1997).
- 28) N. Shibata and K. Ueda, *J. Phys.: Condens. Matter* **11**, 4289 (1991).
- 29) F. F. Assaad, *Phys. Rev. Lett.* **83**, 796 (1999).
- 30) J. Otsuki, H. Kusunose, and Y. Kuramoto, *J. Phys. Soc. Jpn.* **78**, 014702 (2009); *J. Phys. Soc. Jpn.* **78**, 034719 (2009).
- 31) J. Otsuki, H. Kusunose, and Y. Kuramoto, *Phys. Rev. Lett.* **102**, 017202 (2009).
- 32) C. Thomas, A. S. da Rosa Simões, J. R. Iglesias, C. Lacroix, N. B. Perkins, and B. Coqblin, *Phys. Rev. B* **83**, 014415 (2011).
- 33) C. Thomas, A. S. da Rosa Simões, C. Lacroix, J. R. Iglesias, and B. Coqblin, *J. Magn. Magn. Mater.* **372** (2014).
- 34) M. Koga, G. Zaránd, and D. L. Cox, *Phys. Rev. Lett.* **83**, 2421 (1999).
- 35) S. R. White, *Phys. Rev. Lett.* **69**, 2863 (1992); *Phys. Rev. B* **48**, 10345 (1993).
- 36) E. Dagotto, T. Hotta, and A. Moreo, *Phys. Rep.* **344**, 1 (2001).
- 37) M. A. Ruderman and C. Kittel, *Phys. Rev.* **96**, 99 (1954).
- 38) T. Kasuya, *Prog. Theor. Phys.* **16**, 45 (1956).
- 39) K. Yosida, *Phys. Rev.* **106**, 893 (1957).
- 40) J. Friedel, *Phil. Mag.* **43**, 153, (1952).
- 41) M. Yamanaka, M. Oshikawa, and I. Affleck, *Phys. Rev. Lett.* **79**, 1110 (1997).
- 42) M. Oshikawa, *Phys. Rev. B* **84**, 3370 (2000).
- 43) T. Misawa, J. Yoshitake, and Y. Motome, *Phys. Rev. Lett.* **110**, 246401 (2013).
- 44) H. Katsura, *J. Phys. A: Math. Theor.* **45**, 115003 (2012).